Application of regional climate models to the Indian winter monsoon over the western Himalayas

A.P. Dimri [a,*], T. Yasunari [b], A. Wiltshire [c], P. Kumar [d], C. Mathison [c], J. Ridley [c], D. Jacob [d]

[a] School of Environmental Sciences, Jawaharlal Nehru University, New Delhi, India
[b] Hydrospheric Atmospheric Research Center, Nagoya University, Nagoya, Japan
[c] Met Office Hadley Centre, Fitzroy Road, Exeter, Devon, EX1 3PB, UK
[d] Max Planck Institute for Meteorology, Hamburg, Germany

HIGHLIGHTS

► Study provide RCMs' sensitivity towards Indian Winter Monsoon.
► Uncertainty associated with RCMs towards Indian Winter Monsoon.
► Suitability for usage of hydrological/glaciological studies.

ARTICLE INFO

ABSTRACT

The Himalayan region is characterized by pronounced topographic heterogeneity and land use variability from west to east, with a large variation in regional climate patterns. Over the western part of the region, almost one-third of the annual precipitation is received in winter during cyclonic storms embedded in westerlies, known locally as the western disturbance. In the present paper, the regional winter climate over the western Himalayas is analyzed from simulations produced by two regional climate models (RCMs) forced with large-scale fields from ERA-Interim. The analysis was conducted by the composition of contrasting (wet and dry) winter precipitation years. The findings showed that RCMs could simulate the regional climate of the western Himalayas and represent the atmospheric circulation during extreme precipitation years in accordance with observations. The results suggest the important role of topography in moisture fluxes, transport and vertical flows. Dynamical downscaling with RCMs represented regional climates at the mountain or even event scale. However, uncertainties of precipitation scale and liquid–solid precipitation ratios within RCMs are still large for the purposes of hydrological and glaciological studies.

© 2013 Elsevier B.V. All rights reserved.

1. Introduction

Spatiotemporal distribution of precipitation due to orographic forcing and land use/land cover variability is important for assessing regional climates, water recharge, agriculture, and tourism over the western Himalayas (WH). Previous studies suggest that orographic forcing due to the elevation in mountainous regions has a fundamental role in determining the amount of precipitation. In such regions, land use (or land surface conditions) and topography are two key factors in defining the regional climate and its changes (Fyfe and Flato, 1999; Im et al., 2010). These are also some of the most sensitive and vulnerable areas for climate change (Beniston et al., 1997; Beniston, 2003). Altitudinal variations over mountains give rise to sharp gradients of vertical change in the temperature lapse rate (Barry, 2008;

Thayyen et al., 2005). The role of land use and its impact on regional climates and associated precipitation regimes have been studied extensively (Steiner et al., 2009; Fairman et al., 2011; Nair et al., 2011; Przekurat et al., 2011). Precipitation over mountainous regions primarily depends on the source of the moisture that is advected into the region (Viste and Sorteberg, 2011) and the interaction with the prevailing land use (Steiner et al., 2009; Dimri and Niyogi, 2012; Dimri, 2012) and topography (Dimri, 2009; Im et al., 2010). Over mountainous regions, land use and topography can affect surface processes such as snow formation and melting, mostly due to local snow-albedo feedback mechanisms. Previous studies have recognized the complexity associated with precipitation over mountainous regions, which may aid our understanding of the spatial complexity of regional climate variabilities at fine resolutions in these areas. To deal with such a marked elevation dependency within the framework of regional model studies, explicitly representing the interactions between surface variables and the underlying topography is essential (Leung and Ghan, 1995; Qian et al., 2009).

* Corresponding author at: School of Environmental Sciences, Jawaharlal Nehru University, New Delhi, 110067, India. Tel.: +91 11 26704319.
E-mail address: apdimri@hotmail.com (A.P. Dimri).

Various analyses pertaining to the uncertainty/sensitivity of regional climate models (RCMs) in reproducing current climate and associated precipitation during the Indian summer monsoon have been undertaken (e.g., Bhaskaran et al., 1996, 1998, 2012; Saeed et al., 2012). The dependency of precipitation on topography forcing in RCM simulations has also been studied (Takahashi et al., 2010; Im and Ahn, 2011; Gutmann et al., 2012; Schomburg et al., 2012). However, no such studies on the complex topography of the WH during winter (December, January, and February: DJF; hereafter, Indian winter monsoon: IWM) are available. During the IWM, almost 30% of annual precipitation is received over the western Himalayan region. The main sources of this precipitation are eastward-moving synoptic weather systems, known locally as western disturbances (WDs) (Dimri and Mohanty, 2009). This accumulated precipitation, in the form of snow, is very important for the northern Indian region. It provides spring/summer snow melt as river discharge for northern Indian rivers, which support irrigation for agriculture across northern India. An understanding of the IWM is also important for various river-basin hydrological budgets and glacier studies. Therefore, the present study illustrates the role of two available RCM simulations over an eighteen year (1990–2007) period to assess the uncertainty/sensitivity of RCMs in defining the IWM. The downscaled fields were first compared against the corresponding observational reanalyses over the WH, and then a RCM simulation was verified to determine whether it could reproduce the interannual variability (IAV) over the WH. This was then followed by a case study of an active WD to illustrate the robustness of a RCM over a mountainous region for a WD event, and to illustrate the interaction of existing topography with large scale synoptic flow and subsequent precipitation.

In the present paper, the study area, model, and data sets used are discussed in Section 2 and the results are discussed in Section 3; Section 4 briefly introduces the issue of uncertainties associated with RCMs and, finally, Section 5 presents the salient findings of the study and our conclusions.

2. Model and observations

Due to the important and urgent issues regarding changes in the water budget/cycle associated with changes in Indian summer and winter monsoons and their impact on the recent retreat of Himalayan glaciers, the European Union (EU) has sponsored a multi-institutional research project, referred to as the Himalayan Glacier Retreat and Changing Monsoon Pattern (HighNOON). In this program, two RCM simulations were prepared: first, the Meteorological Office Hadley Centre Regional Climate Model version 3 (HadRM3) (Buonomo et al., 2007) upgraded to include the MOSES 2.2 land-surface scheme (Essery et al., 2003), and second, the Regional Model from the Max Planck Institute for Meteorology (REMO) (Jacob et al., 2007). The models were simulated using global ERA-Interim reanalysis data (Dee et al., 2011) to supply large-scale boundary conditions (LBCs). The RCMs are an important tool for providing fine-scale climate information accounting for regional feedback, physical processes, and dynamic forcing. In the present study, the performance of these RCMs was examined to study the IWM and its associated interannual variability. These models have similar LBCs, with the exception of topography. HadRM3 uses the 1984 US Navy data set to specify orography, which contains global elevation data at 10 arc-min resolution. Each 10 min × 10-min area contains modal, maximum, and minimum elevations, orientation of ridges, terrain characteristics, and urban development. REMO uses the GTOPO30 topography data of the US Geological Survey (USGS). The model domain and topography used in the present study are shown in Fig. 1a for HadRM3 and Fig. 1b for REMO. The domains were chosen to cover the whole area of India including the Himalayas. Both the HadRM3 and REMO RCMs simulated the regional climate with a spatial resolution of 0.23° (~25 km). It is important to mention it here that models have similar spatial
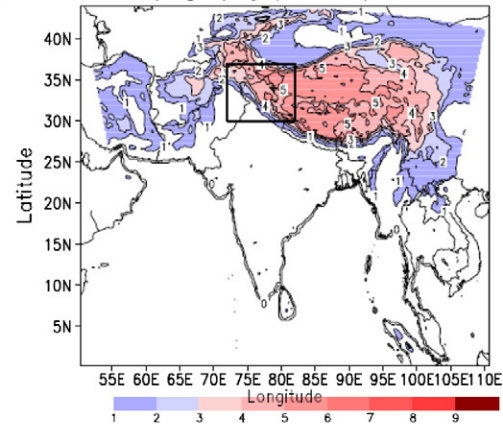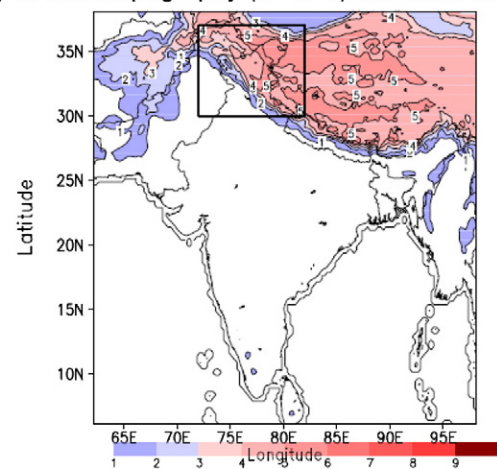
Fig. 1. Topography (*1e − 3 m: shade) and full model domain as used in (a) HadRM3 and (b) REMO. The region under the black box is the western Himalayan region considered in the study. (For interpretation of the references to color in this figure legend, the reader is referred to the web version of this article.)

resolution. But they use different topography having different resolutions. Hence it is key issue that how much topography is smoothened over the spatial horizontal model domain. Due to the difference in the topographic resolution smoothening of the topography in these two models will be different though they are having similar spatial horizontal model resolution. This smoothening of topography will be a key factor in defining the precipitation mechanism over the complex Himalayan topographical region, which is discussed in details in succeeding relevant section. Corresponding model physics,

Table 1
Model design and characteristics used in the present study.

	HadRM3	REMO
Nonhydrostatic	No	No
Grid size	114 × 92	151 × 109
Vertical levels	19	27
Buffer zone	8 cells	8 cells
Spatial resolution	0.23° (~25 km)	0.23° (~25 km)
Land surface scheme	MOSES 2.2 (Essery et al., 2003)	Rainfall runoff scheme (Hageman and Dümenil, 2003)
Convection scheme	Mass flux (Gregory and Rowntree, 1990)	Mass flux (Tiedtke, 1989)
Microphysics	Smith (1990)	Nording (1994) and Sundqvist (1978)

parameterization schemes, and further details used in the model simulations are provided in Table 1.

The simulations were made for a continuous eighteen year period from 1990 to 2007. Atmospheric variables from the ERA-interim reanalysis were provided as input and six-hourly boundary conditions at each atmospheric level were used for both RCMs. Sea-surface temperatures taken from ERA-40 were used in the models. Model results were verified using the corresponding ERA-Interim reanalysis, while
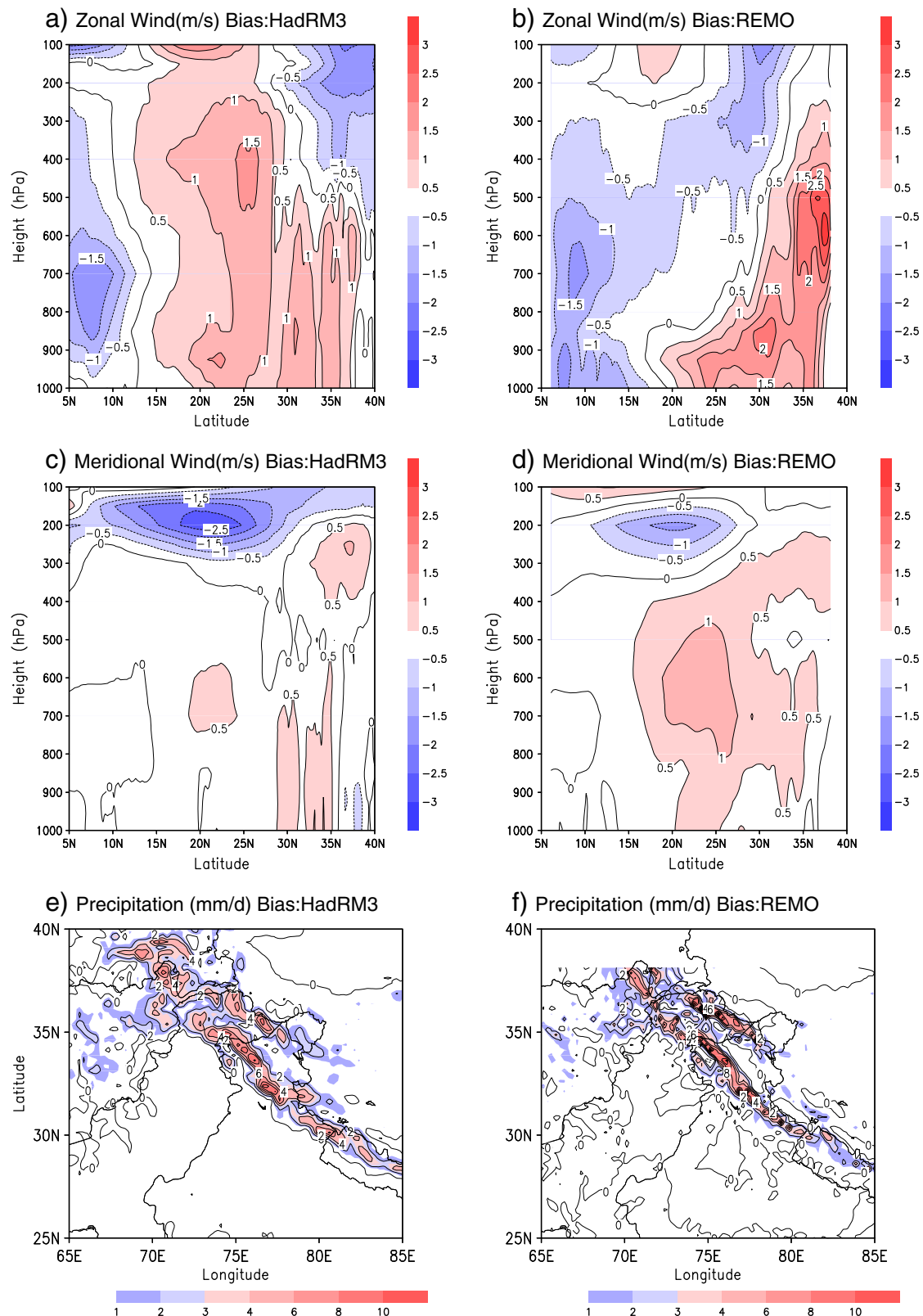
Fig. 2. Latitude–height cross-sectional distribution of model bias for 3-month (DJF) averaged zonal and meridional winds, averaged over 65°–85°E in HadRM3 (a and c) and REMO (b and d). Model bias for 3-month (DJF) averaged precipitation (mm/day) in (e) HadRM3 and (f) REMO regional model.

the precipitation fields were compared using APHRODITE (Yatagai et al., 2009), GPCP (Xie et al., 2003), GPCC (Schneider et al., 2008), and CRU (Mitchell and Jones, 2005) observational gridded data sets. Note that the western Himalayan region has a limited observational network and therefore most of the available reanalyses are based on the assimilation of satellite measurements, upper-air observations, and limited ground observations. Furthermore, the numbers of stations per grid cell are available for APHRODITE and GPCC. This information was used to determine to what extent the gridded precipitation was determined from station data or derived using an interpolation between the stations. GPCP uses satellite measurements and an algorithm for preparation of the data sets. The climate over the WH is colder and drier than that of

other Himalayan regions, and therefore the daily time resolution of APHRODITE is more reliable than the monthly time resolution of other data sets.

3. Results and discussion

3.1. Model sensitivity

For RCMs to be suitable tools for downscaling from global models and subsequent analyses, they must reproduce the climatology of the seasonal (DJF) circulation and its precipitation. The model biases in
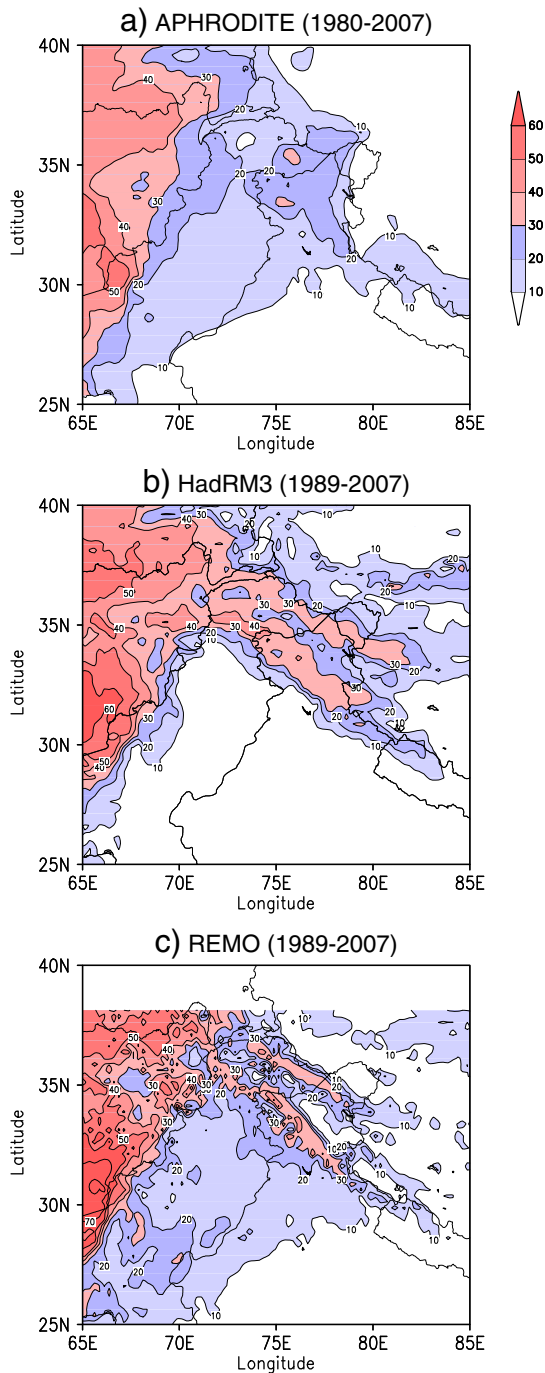
Fig. 3. Ratio of 3-month (DJF) averaged precipitation (mm/day) to the annual averaged precipitation based on observational reanalysis, (a) APHRODITE (1980–2007), and regional models; (b) HadRM3 (1989–2007) and (c) REMO (1989–2007).
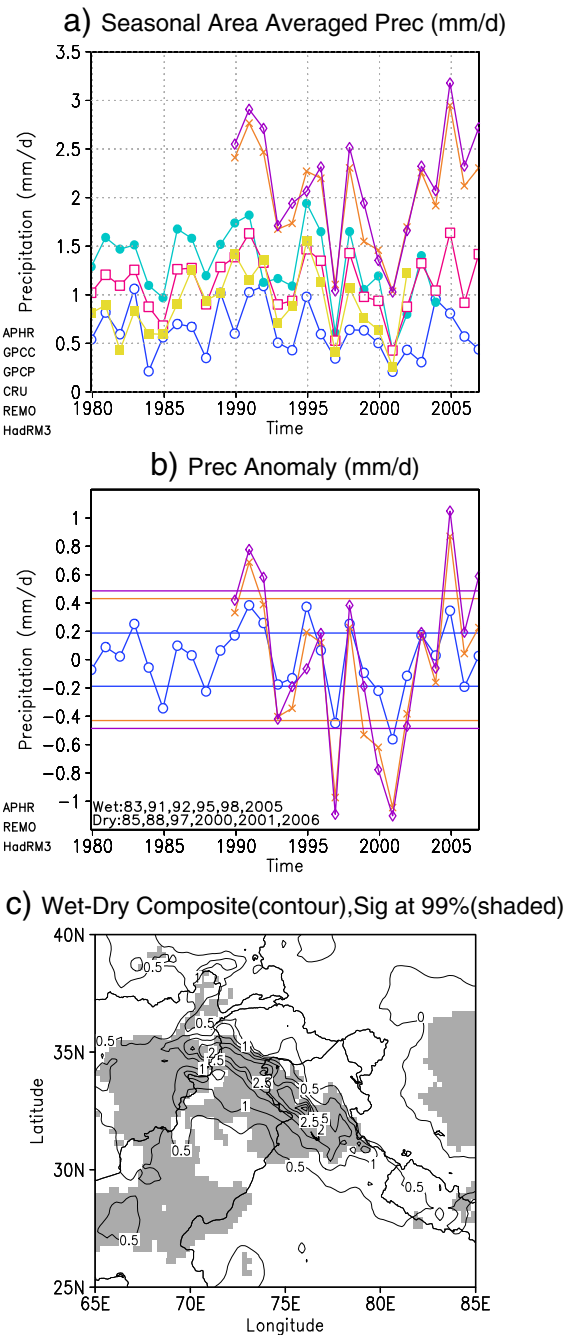
Fig. 4. (a) Interannual variability for 3 months (DJF) in area (30°N 72°–7°N 82°E, as marked in Fig. 1) average precipitation (mm/day); (b) seasonal precipitation (mm/day) anomaly in observational reanalysis (APHRODITE) and regional models (HadRM3 and REMO); (c) APHRODITE observational precipitation differences between 3-month average (DJF) wet- and dry-year composites (contours correspond to differences (wet–dry) and shaded portions correspond to significant regions at the 99% confidence level).

the wind and precipitation components are shown in Fig. 2. The zonal wind components for HadRM3 (Fig. 2a) and REMO (Fig. 2b) show different maxima zones of model bias. In the case of HadRM3, westerly biases dominate ~25°–35°N and persist up to the upper troposphere, and two zones of easterly bias ~700 hPa at 7°N in the lower/mid troposphere and ~200 hPa at 37°N are also observed. In the case of REMO simulations, an easterly bias at 7°N was found to be very similar to that of the HadRM3 simulations. However, one zone of westerly and another zone of easterly bias were identified at different locations. The only major difference between the two climatologies was that HadRM3 produced a uniform westerly bias in the direction, which was not observed in the REMO simulation. In the case of meridional wind component biases (Fig. 2c and d), both models produced similar simulations. In both simulations, similar southerly biases in the lower to mid-troposphere and an upper level northerly bias dominated. Model biases ~100 hPa may be due to upper boundary forcing. Apart from the physical forcing, the differences between the model biases could also be due to the models' internal variability (Giorgi and Bi, 2000). The different schemes used in the model dynamics may provide dissimilar forcing to the models' physics and dynamics. Furthermore,

Fig. 2a and b suggests that winds below the mid-troposphere were slower than the upper troposphere above it. These westerlies had two maxima: one at a lower level and a secondary maxima in the mid-troposphere. The difference in surface boundary forcing due to the Himalayan topography could be one reason for these model biases, which would be dependent on how topography is represented in the model. Localized meso/microscale circulation due to topography can also modulate large-scale flow. Therefore, to understand these biases, one must know how far an air mass is orographically lifted by the topography (Sarkar, 1966; Rhea, 1978). Such disturbances exert an important control, acting either as barriers, elevated heat sources and sinks, or as concentrated areas of high orographic roughness (Sawyer, 1956; Smith, 1979; Barros and Lettenmaier, 1994). These issues particularly topographic forcings were studied and are illustrated using a case study in the following section. In addition, model biases in the precipitation fields were analyzed and are presented in Fig. 2e and f for HadRM3 and REMO, respectively. In both cases, a similar spatial structure in precipitation bias was observed. Both of these figures show multiple zones, with maxima of precipitation associated with the west to east topographic variation in the ridge–valley–ridge–valley structure of the Pir Panjal–Greater Himalayas–Zanskar–Ladhakh–
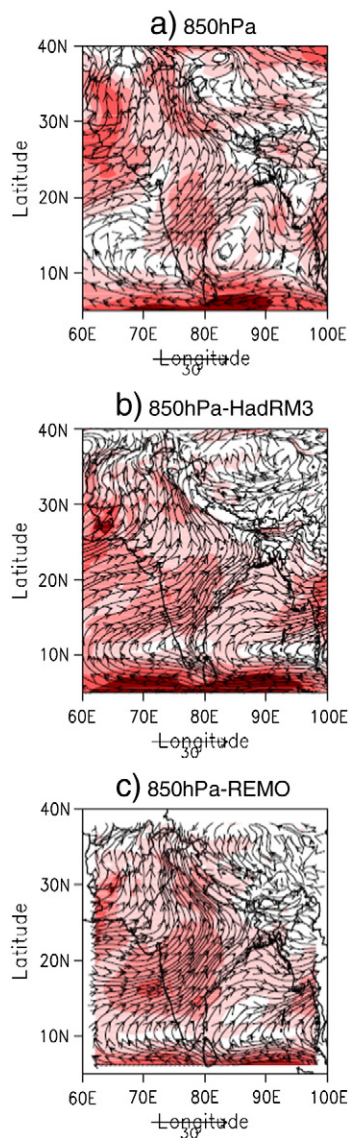
Fig. 5. Difference between 3-month average (DJF) wet- and dry-year composites of wind speed (m/s; shade) and vector wind (m/s; arrow) at 850 hPa in (a) observational data, (b) HadRM3, and (c) REMO. (For interpretation of the references to color in this figure legend, the reader is referred to the web version of this article.)
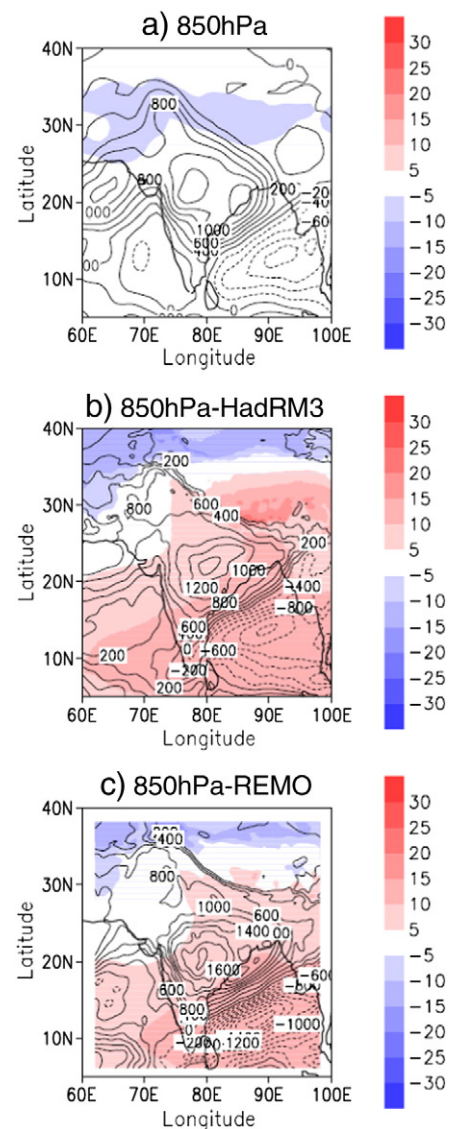
Fig. 6. Same as Fig. 5, but for geopotential height (m; shade) and specific humidity (*1e−6 kg/kg; contour). (For interpretation of the references to color in this figure legend, the reader is referred to the web version of this article.)

Karakoram ranges. Both model simulations indicated a wet bias over the higher elevation regions, but over the plain regions of the Indian subcontinent, the models performed better. It should be noted here that due to the lower number of observations over the mountainous region represented within the precipitation reanalyses field (APHRODITE), there could be an under-representation of the precipitation scale over the mountainous region as compared to plain regions. The role of the Himalayan topography was clear in these model simulations (Dhar and Rakhecha, 1980). The observed precipitation bias over the WH could be enhanced by the lack of a gauge under-catch correction in the measurements, which is likely to be an important issue over the western Himalayan region. This could be assessed based on the station density used in the preparation of precipitation in GPCC and APHRODITE. Roe et al. (2003) performed an experiment that suggested a possible mechanism, which is more apt for such topographic situations, wherein a model cannot capture the full complexities of orographic precipitation. Over narrow mountain peaks, the precipitation maxima occur in the upslope region, whereas over tall and broad mountain regions the precipitation maxima tend to be displaced away from the mountain peaks (Smith, 1979; Alpert, 1986). It is these flows that can determine the potential of strengthening/weakening of horizontal moisture gradients over narrow regions within the planetary boundary layer (McGuire, 1962; Peckman and Wicker, 2000; Medina et al., 2010). To summarize, precipitation biases on the eight grid points around each grid location (i.e., a smoothening) are

averaged and analysis of which showed similar biases in both regional simulations. These corresponded to the basic principle of the formation of precipitation in narrow and/or wide regions of valley bottoms and ridges in the WH.

The ability of RCMs to reproduce regional precipitation patterns was assessed against APHRODITE observations through the seasonal (DJF) to annual precipitation ratio (Fig. 3). The principal distribution was similar over the western Himalayan region, with a similar spread in the spatial pattern across both simulations. Two regions (~36°N 77°E and ~34°N 76°E) had the same ratio of seasonal to annual precipitation maxima in APHRODITE observations as seen in RCM simulations. These zones of maxima were higher in the RCM simulations and were spread along the topographic distribution (Fig. 1). These higher ratios could have resulted from inherent wet model biases (Fig. 2e and f). The wet precipitation biases were oriented over two mountain ridges, which received high precipitation, with the valleys in between receiving lower precipitation. Orographic forcing, either upslope or downslope of the valley floor, contributes to the amount of precipitation. Elevation at a point location displaces the streamlines and changes the distribution of perturbation in vertical velocity with height, which determines the amount of precipitation (Sarkar, 1966, 1967; Schermerhorn, 1967). A detailed analysis showed that for upslope flow, the RCM simulated higher precipitation than was the case in the corresponding observation (Dimri, 2004, 2009). This higher amount of precipitation could still be resultant of interaction
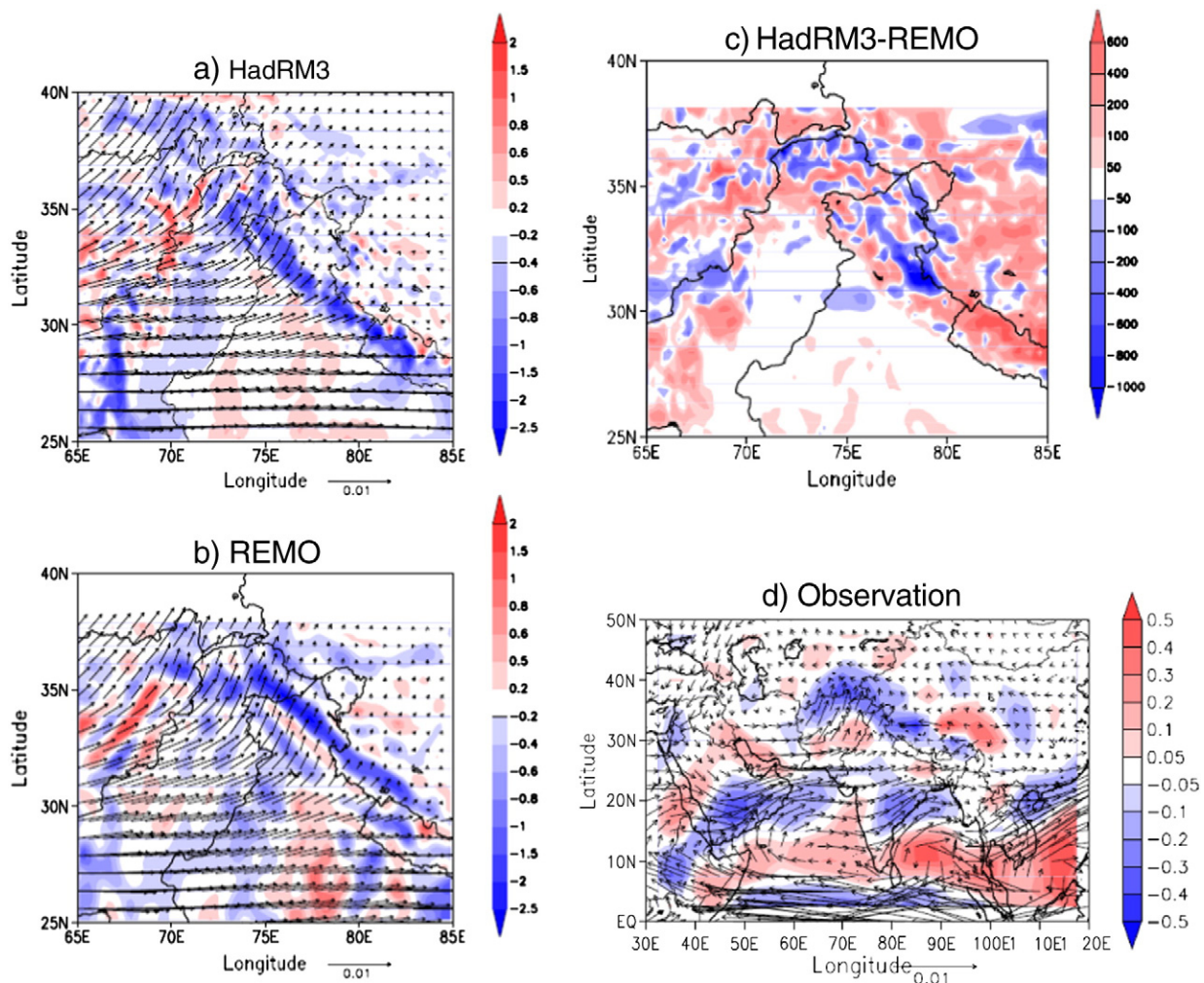
Fig. 7. The difference between 3-month average (DJF) wet- and dry-year composites of vertical integrated moisture flux divergence (*1e − 8 m/s; shade) and transport (arrow) in (a) HadRM3, (b) REMO, and (c) the differences between HadRM3 and REMO topography. (For interpretation of the references to color in this figure legend, the reader is referred to the web version of this article.)

of model topography (smoothened one) with surface drag, flow and upper level circulations. Slope and aspect of surface topography too could also be a part in defining precipitation. These interpretations are provided in succeeding paragraphs.

3.2. Interannual variability

In the previous section, the RCMs were shown to reproduce the climatologies of winter circulation and precipitation over the WH reasonably well, although precipitation in the Himalayan mountain ranges may have been overestimated. In this section, we examine how the RCMs also reproduce the IAV of winter circulation patterns and precipitation. Fig. 4a illustrates the area (30°N, 72°E to 37°N, 82°E: as marked in Fig. 1a and b) — averaged precipitation for four observational data sets and the two RCMs. This region was chosen because it receives the highest amount of winter precipitation in the WH (data not shown). All observation data sets and RCM simulations showed a similar temporal interannual variability, although the amounts of simulated precipitation differed from the observed precipitation. This difference in precipitation could have occurred due to two reasons: the representation of physical and dynamic processes in the model and the representation of catchment observations in the reanalysis. These issues are elaborated in the following paragraphs.

To investigate the RCM precipitation results further, a direct comparison of APHRODITE data with each RCM is presented as a precipitation anomaly in Fig. 4b. APHRODITE was chosen because this observational analysis was available at a comparable resolution to the RCMs and was at a higher resolution than the other available precipitation products. The area-averaged precipitation from the APHRODITE project data shows very high correlations of almost 0.8 with those from GPCC, GPCP, and CRU data. Fig. 4b illustrates that similar patterns of interannual variability are evident in both the RCMs and the observations. Since the RCMs have a wet bias over the WH, they exhibit larger variations than the observed data. Despite this, interannual variability, including years of excess or deficit precipitation, corresponds well in both the model simulations and the observations (Fig. 4b).

Therefore, the model physics and dynamics have been shown to capture the natural IAV over the western Himalayan region. Based on a ±0.5 standard deviation (SD) in the observation fields, 1983, 1991, 1992, 1995, 1998, and 2005 were defined as wet years and 1985, 1988, 1997, 2000, 2001, and 2006 were designated as dry years. Precipitation and circulation fields were composited for these wet and dry years. In the following paragraph, we discuss whether the RCMs were able to reproduce the large-scale fields in their downscaled outputs. First, Fig. 4c presents the difference between the composite wet and dry precipitation years, with statistical significance indicated by the hatched (shaded) regions. Apart from receiving higher precipitation, the western Himalayan region shows a significant difference between wet and dry years at the 99% confidence level.

Analysis of the composite circulation fields indicated a reasonably good performance by the RCMs. Fig. 5 illustrates the difference in seasonally averaged 850-hPa wind speeds and directions between wet and dry composites. Fig. 5a–c corresponds to the global observation reanalysis data set (ERA-Interim), HadRM3, and REMO, respectively. In the lower troposphere at 850 hPa, during wet years, the observed strong winds over the central Indian region are well represented by the RCM simulations, as well as weak westerlies south of 10°N. The RCM simulations also represent the stronger lower-tropospheric meridional wind shear during wet year composites well. This is important for assessing the synoptic "surface low" formation, which generates conditions conducive for high precipitation. Considering first the circulation for wet years, the mid-troposphere circulation at 500 hPa (data not shown) is influenced by Himalayan topography, which generates strong westerlies over central India and a pronounced north–south wind shear occurs. This was reproduced by the RCM simulations.

Similarly, the observed variability in circulation fields during wet and dry years was also captured by RCMs at 200 hPa. Models must represent large-scale features well while downscaling to allow an understanding of the associated weather. To investigate the variability associated with geopotential height and specific humidity, wet- and dry-year composites were examined as shown in Fig. 6. The lower troposphere exhibited a similar distribution of deficit and excess specific humidity during composites of the extreme years. During wet years, low (high) specific humidity was observed over the Bay of Bengal (Indian subcontinent) in both the observed (Fig. 6a) and simulated fields (Fig. 6b and c). A similar distribution with a core of maxima/minima was seen over central India/Bay of Bengal. The geopotential differences in wet- and dry-year composites show that the weaker geopotential over and along ~30°N by RCMs was well simulated, although with a much stronger geopotential over the Indian subcontinent. For the corresponding distribution in the mid-troposphere at 500 hPa, the RCM simulations produced a similar spread in geopotential but with slightly higher values (figures not shown). Over the northwest Indian subcontinent, especially over Afghanistan and Pakistan, the RCMs simulated a weaker geopotential during wet years than dry years, as seen in the corresponding observations. The specific humidity distribution, with a core of maxima/minima, was well simulated in the mid-troposphere by both RCMs. In the upper troposphere at 200 hPa, a similar pattern of geopotential distribution in the different wet- and dry-year composites was observed (figure not shown). The eighteen year RCM simulations did represent the spatial variability in the geopotential fields but the variability was a little greater than in the observed data. The
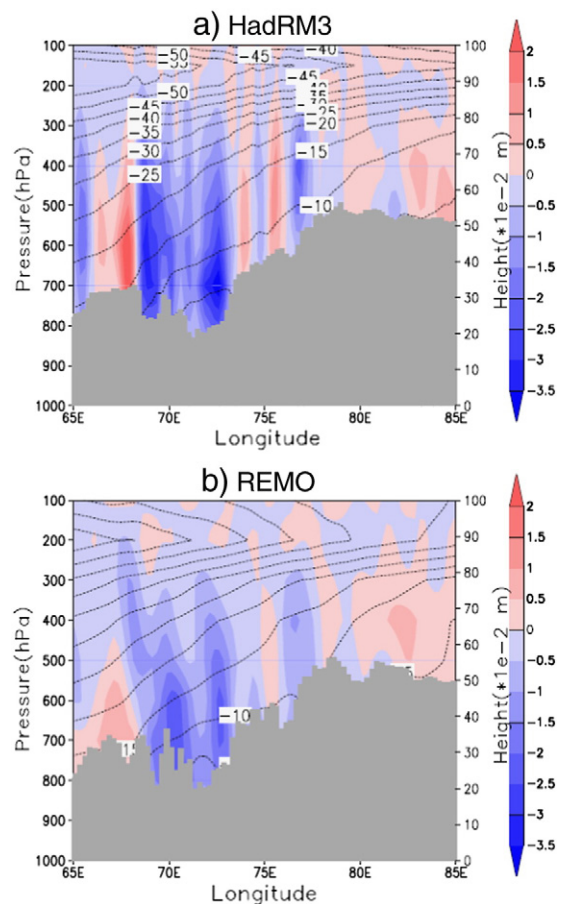
Fig. 8. Longitude–height distribution of the differences between 3-month average (DJF) wet- and dry-year composites of vertical velocity (hPa/s; shade) and geopotential height (m; broken contour) in (a) HadRM3 and (b) REMO at 35°N latitude. Right-hand vertical axis corresponds to topography (*1e−2 m). (For interpretation of the references to color in this figure legend, the reader is referred to the web version of this article.)

variability of specific humidity variability was well reproduced in the RCM simulations.

We now examine the impact of the different topographic representations adopted in the two RCMs. Note that both RCMs are forced with differences in topography. Fig. 7a and b presents seasonal mean vertical integrated moisture vapor fluxes and the transport difference between wet and dry years composited in HadRM3 and REMO simulations. The two RCM simulations showed similar large-scale moisture fluxes, with stronger transport from westerly directions. High flux convergence occurred over and across high topographical regions, while weaker flux convergence or even divergent fluxes were seen over and along valley regions. Further investigation indicated a shift of convergence and divergence zones in the model simulations. This observed shift between the two simulations could have been due to the different topography used as a surface boundary. Fig. 7c shows the difference between HadRM3 and REMO topography. This difference results in different forcing over the Himalayan region (Fig. 7a and b). Both simulations show that the high altitude (mountainous) regions correspond to convergence zones, and the lower altitude (valley) regions correspond to divergence zones. Moisture flux transport and convergence/divergence zones as seen in the corresponding observations are presented in Fig. 7d. Spatial distribution
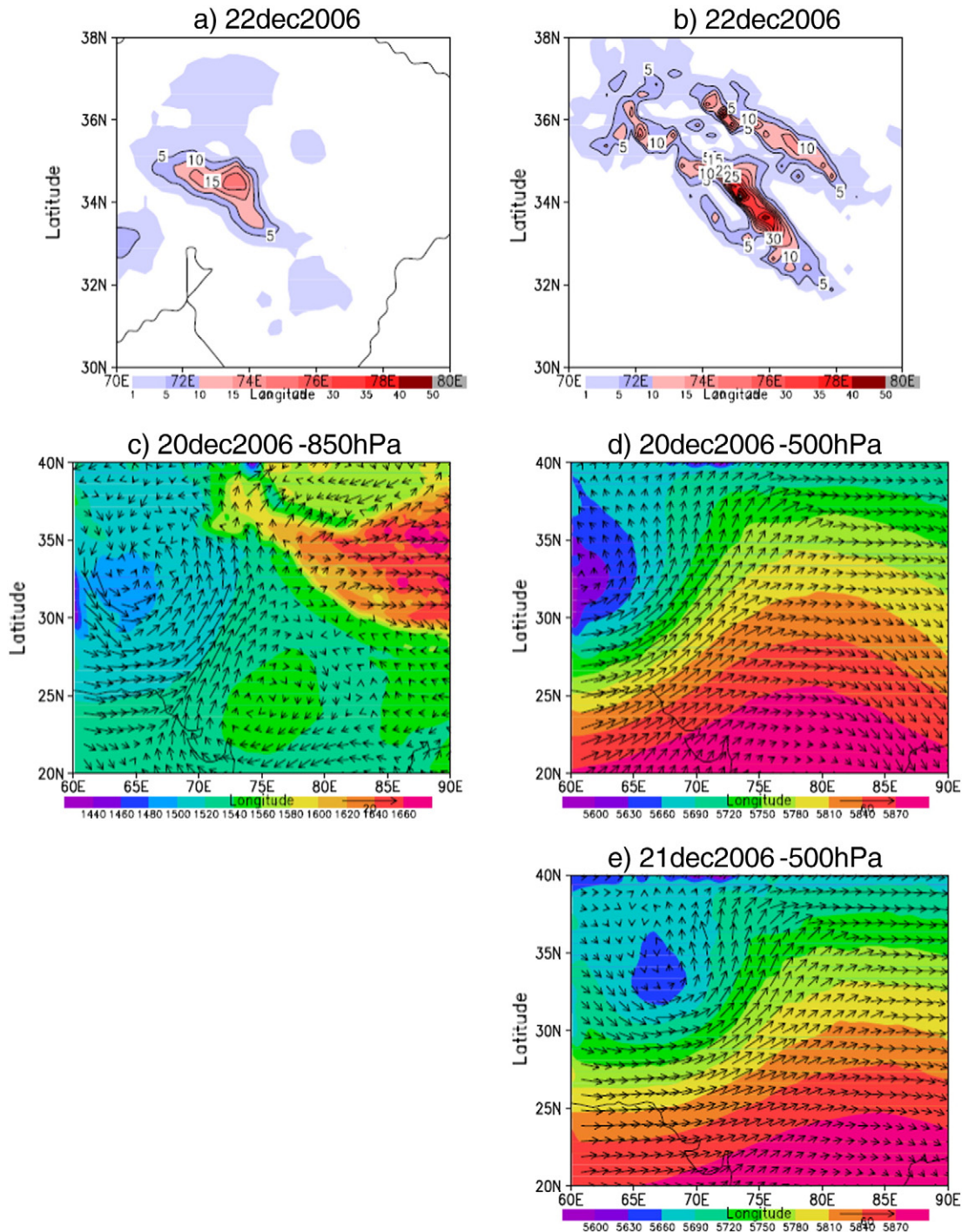
Fig. 9. Twenty-four hour cumulative precipitation on 22 December 2006 in (a) observational data (APHRODITE) and (b) the corresponding REMO simulated field, and geopotential height (m; shade) and vector wind (m/s; arrow) in the REMO simulation at (c) 850 hPa on 20 December 2006, (d) 500 hPa on 20 December 2006, and (e) 500 hPa on 21 December 2006. (For interpretation of the references to color in this figure legend, the reader is referred to the web version of this article.)

in composite analysis was similar but with less detail than in the RCMs due to the coarser resolutions of observed reanalysis fields. To illustrate this further, Fig. 8 indicates longitude, height vertical cross section of the composite vertical velocity (shaded), and geopotential

height difference (contour) between wet and dry years. The topographies used in the two RCM simulations are also shown (in the gray shaded bar). In both cases, the vertical velocity maxima are always either along the upslope side of topography or over the valley bottom,
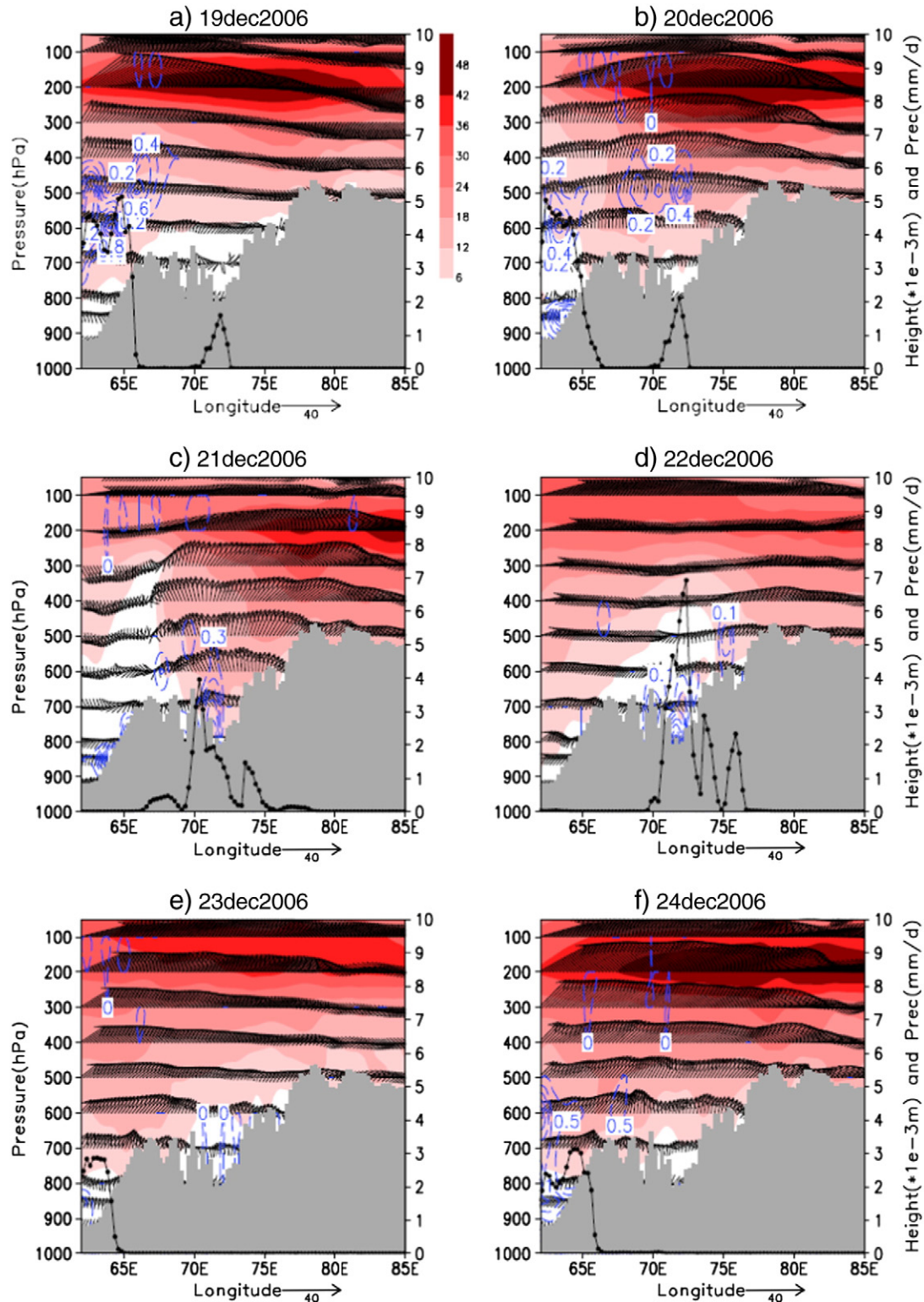
Fig. 10. Longitude–height distribution of liquid water content (*1e − 5 kg/kg; blue broken contour), wind speed (m/s; shade), and wind direction (m/s; arrow); observed precipitation (mm/day; black contour) and topography (*1e − 2 m; shaded bar) on (a) 19 December 2006, (b) 20 December 2006, (c) 21 December 2006, (d) 22 December 2006, (e) 23 December 2006, and (f) 24 December 2006 at 35°N latitude in the REMO simulation. Right-hand vertical axis corresponds to topography (*1e − 3 m) and precipitation (mm/day). (For interpretation of the references to color in this figure legend, the reader is referred to the web version of this article.)

which shows that the influence of the ridge–valley system on the vertical motion (and precipitation formation processes) is evident. Even relatively minor ridge–valley undulations at altitudes ~4 km gave rise to orographic uplift and triggered vertical motions that extended to the upper troposphere. These marked vertical distributions across the Himalayan region provide a mechanism for generating more precipitation during wet years than dry years. This composite analysis of the difference of seasonally averaged geopotential height between wet and dry years strongly suggests that the decrease (increase) in the change in the upper tropospheric circulation is crucial for more (less) precipitation across the western Himalayan region. The association of enhanced vertical maxima along the upslope
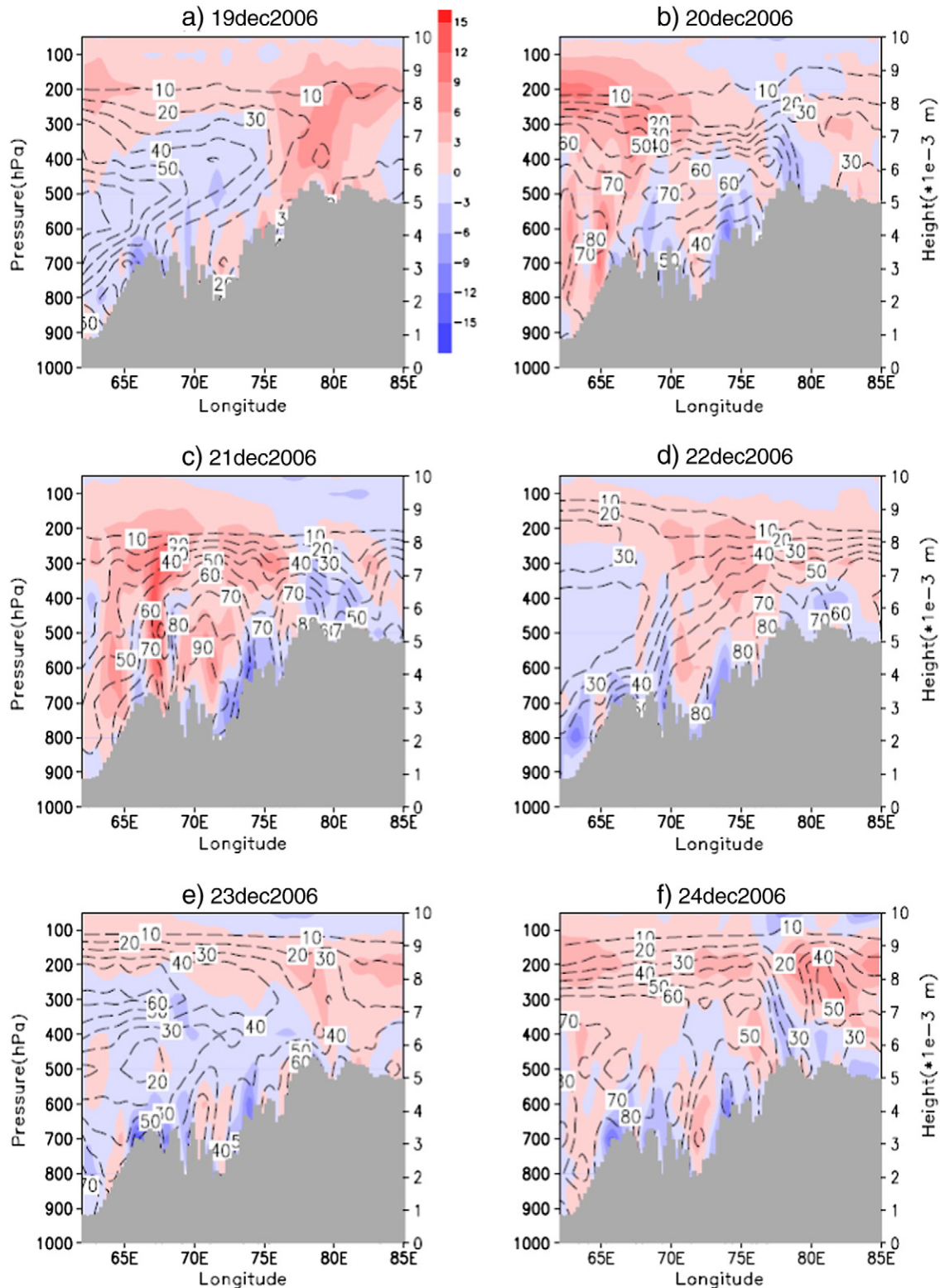
Fig. 11. Same as Fig. 10, but for vorticity (*1e − 5/s; shade), relative humidity (%, broken contour), and topography (*1e − 3 m; shaded bar). (For interpretation of the references to color in this figure legend, the reader is referred to the web version of this article.)

topography and over valley bottoms with reduced geopotential height in the mid- and upper troposphere during wet years provides stronger vertical uplift due to the topography and large-scale dynamic forcing acting together. Such increased vertical motion enhances precipitation during wet years. Characteristic patterns of atmospheric ascent over elevated ground suggest that the two RCM simulations displayed similar physical mechanisms, even under somewhat different depictions of the orography. However, careful scrutiny of the topographic details indicated that relatively minor ridge–valley undulations up to altitudes ~4 km defined the precipitation distribution. The corresponding distribution of precipitation (Fig. 3) and convergence/divergence zones (Fig. 7) illustrates this difference. The characteristic zones of lower elevation are associated with higher precipitation and convergence. Having verified the model processes, we can proceed to a specific case study.

3.3. WD case study

To investigate the interaction of WDs with the Himalayan topography and its related subsequent effects on precipitation-forming mechanisms, an intensive WD (19–23 December 2006; Mausam, 2007) was considered with the intention of assessing the robustness of the RCMs. This analysis was intended to determine the prospect of using dynamic downscaling methods in river basin studies (e.g., hydrological, glacier mass balances) over regions of complex terrain. As explained in Section 1, WDs are synoptic weather systems that deliver much of the winter precipitation over the WH (Dimri and Mohanty, 2009).

The APHRODITE precipitation (24 hour cumulative at 0000UTC on 22 December 2006) shows a show a large daily precipitation event (see Fig. 9a). The corresponding simulated precipitation from REMO is shown in Fig. 9b. In both the model and the observations, the peak precipitation appears across the Himalayan range, with the model showing the wet bias discussed previously. The RCM geopotential height field at 850 hPa (Fig. 9c), shows a well-defined surface low associated with cyclonic circulation over 33°N, 65°E in the northwest of the WH 2 days previously. The system develops on 20 and 21 December 2006 as it moves over the WH (Fig. 9d and e), indicating that such systems can be adequately depicted from the RCM's simulation.

To assess orographic forcing and the precipitation-forming mechanism, a latitudinal (35°N) cross-sectional distribution of liquid water content, winds, precipitation, and topography is presented in Fig. 10. This depicts the maxima of liquid water content peaks either along the upslope/windward topography or over valley floors. On 20, 21, and 22 December 2006 (Fig. 10b–d), when the system was most intense, an increase in vertical columnar liquid water content in the rear of the WD was clear. Such a distribution corresponded with the precipitation distribution. This system advancement was in conjunction with the 200-hPa subtropical westerly jet. During this travel/passage of the storm, storm interaction with local topography shows vertical motion along the upslope/windward side and/or over valley bottoms. Such orographic feedback will force available moisture upward, which will condense and subsequently lead to higher precipitation rates. This is seen in the liquid water content distribution, which increases where topography forces vertical motion. This interaction can be observed during the peaks of the WD on 20, 21, 22, and 23 December 2006 (Fig. 10b–e, respectively). However, this mechanism dominates in lower topographical regions rather than over higher topography.

The vorticity and relative humidity distribution over this period are presented in Fig. 11. The vertical deflection of flow induced by the topography results in adiabatic cooling, and with sufficient moisture forms cloud and eventually precipitation. Convergence on the upslope/windward side due to decreased velocity through orographic retardation will deform or slow down the flow, generating a mid-troposphere

positive vorticity at the peak of the storm (Fig. 11a and b). Higher relative humidity is seen in the regions of positive vorticity (Fig. 11b and c). A weaker negative vorticity occurs along the topographic surface toward the windward side with a positive vorticity over the leeward side and valley floors. The effects of the stronger valley flows are twofold: first, these stronger valley flows reduce upslope moisture flow, and second, the valley boundaries provide conditions for precipitation formation. This suggests the models' robustness for mountainous regions at the event scale.

4. Uncertainty associated with RCMs

We concluded that the RCMs were robust in nature with good modeling outputs over a mountainous region at the event level. However, the results may not be accurate enough for use as an input for hydrological and glaciological studies, cloud burst analysis, or irrigation determination, given that we obtained differences in circulation patterns and precipitation compared to observations. Use of regional model outputs "without tuning" to evaluate glacier responses to climate change in the Himalayan high mountains is still elusive (Yasunari et al., 2012). These issues with the RCM simulations still need to be studied with a more holistic analysis. Recent work by Saeed et al. (2012), although focusing on the summer monsoon (SASM), provided an improved framework for RCMs to capture the fundamental structure of the SASM system. Bhaskaran et al. (2012) represented downscaling at the subregional scale with an RCM simulation and showed that smaller domains may favor frequent moderate uplifting and subsequent precipitation at the daily timescale. Lucas-Picher et al. (2011) using a multi-RCM simulation, arrived at the conclusion that predicted precipitation amounts and regional distribution differ substantially among RCMs due to poor, or no, representation of important feedbacks.

Although most of the studies discussed above considered sensitivity/uncertainty issues of RCMs during the summer monsoon time, the present work provides insights regarding the sensitivity/uncertainty of RCMs during the winter monsoon, together with associated precipitation and temperature. During the winter, having an understanding of the liquid–solid precipitation ratio within the model framework is also important for various hydrological and glaciological purposes. Therefore, the sensitivity of RCMs to this parameter also needs to be evaluated.

5. Conclusions

In this study, we analyzed the output of high-resolution RCM simulations forced at the boundaries by a coarser-resolution reanalysis data. From this output, winter precipitation arising from western disturbances across the WH is depicted. Dynamic downscaling resulting from the use of RCMs has not been discussed previously in terms of such heterogeneous topography and land use conditions. Two RCM simulations were analyzed with a corresponding verification reanalysis, and the regional climate and weather regimes were determined to be realistically simulated over the western Himalayan region. However, the RCMs produced a wet bias over high-elevation sites in the WH, but this may have been associated with the deficit of high-altitude observations. This also could be depending on how physics and dynamics are represented within the model fields. The RCMs reproduced the observed interannual variability, simulating the atmospheric circulation patterns, which allowed the depiction of extreme precipitation events. With a specific reference of a western disturbance, analysis revealed that the RCMs correctly simulated some features of dynamic and orographic forcing and the associated precipitation mechanisms.

However, to assess precipitation thresholds over mountainous regions, particularly for studies of hydrology, and to determine the mass balance of glaciers, much finer downscaling over mountainous

regions is needed, with a simultaneous investigation of model internal variability.

References

Alpert P. Mesoscale indexing of the distribution of orographic precipitation over high mountains. J Clim Appl Meteorol 1986;25:532–45.

Barros AP, Lettenmaier DP. Dynamic modeling of orographically induced precipitation. Rev Geophys 1994;32:265–84.

Barry RG. Chapter 5: regional case studies. Mountain weather and climate. 3rd ed. Cambridge: Cambridge University Press; 2008.

Beniston M. Climatic changes in mountainous regions: a review of possible impacts. Clim Change 2003;59:5-31.

Beniston M, Diaz HF, Bradley RS. Climatic change at higher elevation sites. Clim Change 1997;36:233–51.

Bhaskaran B, Jones RG, Murphy JM, Nouger M. Simulations of Indian summer monsoon using a nested regional climate model: domain size experiments. Clim Dyn 1996;12:573–87.

Bhaskaran B, Murphy JM, Jones RG. Intraseaonal oscillation in Indian summer monsoon simulated by global and nested regional climate models. Mon Weather Rev 1998;126:3124–34.

Bhaskaran B, Ramachandran A, Jones R, Moufouma-Okia W. Regional climate model applications on sub-regional scales over the Indian monsoon region: the role of domain size on downscale uncertainty. J Geophys Res 2012;117:D10113. http://dx.doi.org/10.1029/2012JD017956.

Buonomo E, Jones R, Huntingford C, Hannaford J. On the robustness of changes in extreme precipitation over Europe from two high-resolution climate change simulations. Q J R Meteorolog Soc 2007;133:65–81.

Dee DP, Uppala SM, Simmons AJ, Berrisford P, Poli P, Kobayashi S, et al. The ERA-interim reanalysis: configuration and performance of the data assimilation system. Q J R Meteorolog Soc 2011;137:553–97.

Dhar ON, Rakhecha PR. The effect of elevation on monsoon rainfall distribution in the Central Himalayas. In: Lighthill J, Pearce RP, editors. Monsoon dynamics. Cambridge University Press; 1980. p. 253–60.

Dimri AP. Impact of horizontal model resolution and orography on the simulation of a western disturbance and its associated precipitation. Meteorol Appl 2004;11:115–27.

Dimri AP. Impact of subgrid scale scheme on topography and landuse for better regional scale simulation of meteorological variables over the western Himalayas. Clim Dyn 2009;32:565–74.

Dimri AP. Wintertime land surface characteristics in climatic simulations over the western Himalayas. J Earth Syst Sci 2012;121(2):329–44.

Dimri AP, Mohanty UC. Simulation of mesoscale features associated with intense western disturbances over the western Himalayas. Meteorol Appl 2009;16:289–308.

Dimri AP, Niyogi D. Regional climate model application at subgrid scale on Indian winter monsoon over the western Himalayas. Int J Climatol 2012. http://dx.doi.org/10.1002/joc3584.

Essery RLH, Best MJ, Betts RA, Cox PM. Explicit representation of subgrid heterogeneity in a GCM land surface scheme. J Hydrometeorol 2003;4(3):530–43.

Fairman Jr JG, Nair US, Christopher SA, Molg T. Landuse change impacts on regional climate over Kilimanjaro. J Geophys Res 2011;116:D03110. http://dx.doi.org/10.1029/2010JD014712.

Fyfe JC, Flato GM. Enhanced climate change and its detection over the Rocky Mountains. J Climatol 1999;12:230–43.

Giorgi F, Bi X. A study of internal variability of a regional climate model. J Geophys Res 2000;105:29503–21.

Gregory D, Rowntree PR. A mass flux convection scheme with representation of cloud ensemble characteristics and stability dependent closure. Mon Weather Rev 1990;118:1483–506.

Gutmann ED, Rasmussen RM, Liu C, Ikeda K, Gochis DJ, Clark MP, et al. A comparison of statistical and dynamical downscaling of winter precipitation over complex terrain. J Climatol 2012;25:262–81.

Hageman S, Dümenil G. Improving a subgrid runoff parameterization scheme for climate models by the use of high resolution data derived from satellite observations. Clim Dyn 2003;21:349–59.

Im ES, Ahn JB. On the elevation dependency of present day climate and future change over Korea from a high-resolution regional climate simulation. J Jpn Meteorol Soc 2011;89:89-100.

Im ES, Coppola E, Giorgi F, Bi X. Local effects of climate change over the Alpine region: a study with a high resolution regional climate model with a surrogate climate change scenario. Geophys Res Lett 2010. http://dx.doi.org/10.1029/2009GL041801.

Jacob D, Barring L, Christensen OB, Christensen JH, Castro M, Deque M, et al. An inter-comparison of regional climate models for Europe: model performance in present day climate. Clim Change 2007;81:31–52.

Leung LR, Ghan S. A subgrid parameterization of orographic precipitation. Theor Appl Climatol 1995;52:95-118.

Lucas-Picher P, Christensen JH, Saeed F, Kumar P, Asharaaf S, Ahrens B, et al. Can regional climate models represent the Indian monsoon? J HydroMeteorol 2011;12:849–68.

Mausam 2007;58 (4):592.

McGuire EL. The vertical structure of three drylines as revealed by aircraft traverses, 7. National Severe Storms Project Rep; 1962. [11 pp.].

Medina S, Houze Jr RA, Kumar A, Niyogi D. Summer monsoon convection in the Himalayan region: terrain and land cover effects. Q J R Meteorolog Soc 2010;136:593–616.

Mitchell TD, Jones PD. An improved method of constructing a database of monthly climate observations and associated high resolution grids. Int J Climatol 2005;25:693–712.

Nair US, Wu Y, Kala J, Lyons TJ, Pielke Sr RA, Hacker JM. The role of landuse change on the development and evolution of the west coast trough, convective clouds, and precipitation in southwest Australia. J Geophys Res 2011;116:D07103. http://dx.doi.org/10.1029/2010JD014950.

Nording TE. Extended versions of the convective parameterization scheme at ECMWF and their impact on the mean and transient activity of the model in the tropics. ECMWF Tech MemReading, UK: European Centre for Medium-range Weather Forecasts; 1994.

Peckman SE, Wicker LJ. The influence of topography and lower tropospheric winds on dry morphology. Mon Weather Rev 2000;128:2165–89.

Przekurat AB, Pielke Sr RA, Eastman JL, Coughenour MB. Modelling the effects of land-use/land-cover changes on the near surface atmosphere in southern South America. Int J Climatol 2011. http://dx.doi.org/10.1002/joc.2346.

Qian Y, Ghan SJ, Leung LR. Downscaling hydroclimatic changes over the western US based on CAM subgrid scheme and WRF — regional climate simulations. Int J Climatol 2009;30:675–93.

Rhea JO. Orographic precipitation model for hydrometeorological useAtmospheric science paper no. 2870067-0340; 1978. [221 pp.].

Roe GH, Montgomery DR, Hallet B. Orographic precipitation and the relief of mountain ranges. J Geophys Res 2003;108(B6):2315. http://dx.doi.org/10.1029/2001JB001521.

Saeed F, Hagemann S, Jacob D. A framework for the evaluation of the South Asian summer monsoon in a regional climate model applied to REMO. Int J Climatol 2012;32:430–40.

Sarkar RP. A dynamical model of orographic rainfall. Mon Weather Rev 1966;94:555–72.

Sarkar RP. Some modifications in a dynamical model of orographic rainfall. Mon Weather Rev 1967;95:673–84.

Sawyer JS. The physical and dynamical problems of orographic rain. Weather 1956;11:375–81.

Schermerhorn VP. Relations between topography and annual precipitation in western Oregon and Washington. Water Resour Res 1967;3:707–11.

Schneider U, Fuchs T, Meyer-Christoffer A, Rodolf B. Global precipitation analysis products of the GPCP, full data reanalysis product version 4. Global Precipitation Climatology Centre Rep; 2008 [12 pp.].

Schomburg A, Venema V, Ament F, Simmer C. Disaggregation of screen level variables in a numerical weather prediction model with an explicit simulation of subgrid scale land-surface heterogeneity. Meteorol Atmos Phys 2012;116:81–94.

Smith RB. Some aspects of the quasi geostrophic flow over mountains. J Atmos Sci 1979;36:2385–93.

Smith RB. A scheme for predicting layer clouds and their water content in a general circulation model. Q J R Meteorolog Soc 1990;116:435–60. http://dx.doi.org/10.1002/qj.49711649210.

Steiner AL, Pal JS, Rauscher SA, Bell JL, Diffenbaugh NS, Boone A, et al. Land surface coupling in regional climate simulations of the west African monsoon. Clim Dyn 2009. http://dx.doi.org/10.1007/s00382-009-0543-6.

Sundqvist H. A parameterization scheme for non-convective condensation including prediction of cloud water content. Q J R Meteorolog Soc 1978;104:677–90.

Takahashi HG, Yoshikane T, Hara M, Takata K, Yasunari T. High resolution modeling of the potential impact of land surface conditions on regional climate over Indochina associated with diurnal precipitation cycle. Int J Climatol 2010;30:2004–20.

Thayyen RJ, Gregan JT, Dobhal DB. Slope lapse rates of temperature in Din Gad (Dokriani Glacier) catchment, Garhwal Himalayas, India. Bull Glaciol Res 2005;22:31–7.

Tiedtke M. A comprehensive mass flux scheme for cumulus parametrization in large scale models. Mon Weather Rev 1989;117:1779–800.

Viste E, Sorteberg A. Moisture transport into the Ethiopian highlands. Int J Climatol 2011. http://dx.doi.org/10.1002/joc.3409.

Xie P, Janowiak JE, Arkin PA, Adler RF, Gruber A, Ferraro RR, et al. GPCP pentad precipitation analyses: an experimental datasets based on gauge observations and satellite estimates. J Clim 2003;16:2197–214.

Yasunari T, Fujita K, Matsuda Y. Regional model outputs and glacier mass balance. Note for HighNOON project (personal communication); 2012.

Yatagai A, Arakawa O, Kamiguchi K, Kawamoto H. A 44-year daily gridded precipitation dataset for Asia based on a dense network of rain gauges. SOLA 2009;5:137–40.